Stöcklein *et al. Heritage Science* (2022) 10:141
https://doi.org/10.1186/s40494-022-00768-5

Heritage Science

RESEARCH

Open Access

Hygro-mechanical short-term behaviour of selected coatings: experiments and material modelling on vapour permeability and mechanical properties

Josef Stöcklein[1], Daniel Konopka[1], Gerald Grajcarek[1], Oliver Tietze[1], Silvia Oertel[2], Andreas Schulze[2] and Michael Kaliske[1*]

Abstract

Many pieces of fine art are made of wood that has been treated with coatings. Since wood is a very hygroscopic material, the moisture content strongly influences the deformation of wooden parts. Coatings often act as moisture barriers. Therefore, the moisture permeability of coatings must be considered for the evaluation of the structural behaviour. The mechanical properties are also relevant to evaluate the deformation of thin artwork like panel paintings as well as the damage of paintings and varnishes. Therefore, the mechanical properties and the permeability of selected coatings used for cultural wooden artwork are investigated and presented in the article at hand. In this study, coatings of three artworks are investigated: a Lusatian cupboard from the eighteenth century, an altarpiece by L. Cranach the Elder and a Russian icon from 1912. The coatings considered are white ground, colours, varnishes, glue and textile reinforced sizing. Mechanical tests are conducted to evaluate the stiffness and tensile strength of the Russian icon's coating. Cup tests are made to identify the moisture permeability of the coatings. This test was conducted for single coatings as well as for coating systems consisting of different coatings to investigate both the moisture barrier of single coatings and the interaction of coatings. Exponential functions for the relative humidity-dependent permeability are fitted based on the experimental data. The results allow the quantification of permeability for all investigated coatings—from white ground with a high permeability to beeswax with a low permeability—and the magnitude of moisture dependency of the coating's permeability. Furthermore, it is shown that the simple addition of the water vapour resistance of single coatings underrates the resistance of a total coating system. By the mechanical tests, the strength, ultimate strain and Young's modulus are obtained. The permeability and the mechanical parameters are required as input for numerical simulations of the structural behaviour of coated wooden artwork. These results are a good step forward to assess the risk of damage of coated wooden artwork.

Keywords: Coating, Cup test, Furniture, Material modelling, Moisture, Paint, Panel painting, Tensile strength, Water vapour permeability, Water vapour resistance

Introduction

A large number of cultural objects with very high intangible value for future generations are exhibited and placed in storage in museums, churches and other places all over the world. Many artworks are based on constructions of wood, coated with several layers with different properties. These objects include panel

*Correspondence: michael.kaliske@tu-dresden.de

[1] Institute for Structural Analysis, Technische Universität Dresden, 01062 Dresden, Germany
Full list of author information is available at the end of the article

paintings and historical painted cupboards, which are the focus of this article. Mostly, the purpose of these coatings is to yield aesthetic and resistant surfaces. Therefore, the coatings and their properties are especially important for conservation and restoration.

An approach of preventive conservation is the numerical prediction of material and structural behaviour of cultural objects to quantify stresses and the potential of damage occurring due to the boundary conditions. This information can then be used to identify adequate climatic conditions and restoration measurements. Damage occurs especially due to mechanical stress. Due to the hygroscopic character of supporting materials like wood, moisture strongly influences the mechanical behaviour of structures consisting of these materials. Since coatings often significantly resist the water vapour emission, it is necessary to characterise the hygro-mechanical behaviour of both wood and its coatings. For many wood species, the mechanical properties as well as the moisture diffusion, sorption, swelling and shrinking properties have been thoroughly investigated. Regarding coating materials, the need for material research is high since many different coatings have been used over the centuries in the history of painting. Therefore, mechanical properties and the permeability of selected coatings used for cultural wooden artwork are investigated in the study at hand.

Research on the material properties of coatings is already available for different types of coatings and with different research focuses. Mechanical properties can be found in [1–5]. Hygric properties are investigated in [3, 4, 6–11]. Simulation approaches are presented and used in [1, 3, 4, 8, 9, 12, 13]. In [1, 2], the focus is on dimensional changes of coated wood causing stresses by differences in hygroexpansion and stiffness between wood and coating and, therefore, only mechanical and swelling/shrinking properties are investigated for glue, gesso, oil paints, canvas and wood. In [3], the influence of the diffusion process of moisture in wood on the structural behaviour is considered, but only gesso with no significant water vapour resistance is used. For the investigation of this type of stress, the elastic modulus of the coatings is needed, which is investigated in [1–3] partly to be RH- and age-dependent. In [4], elastic moduli of a ground layer of chalk and glue and of oil paints with special focus on ageing are presented. In [5], mechanical properties of coatings are investigated for violin varnishes including the frequency dependency. In the article at hand, the stress–strain relation of two different coating systems related to a historic icon is investigated in order to identify the initial elastic modulus, the strength and the yield strain. These properties are used to fit the parameters of a damage model. Age dependency and dynamic properties are not considered.

Since the structural behaviour of panel paintings and the potential for damage of applied coatings are strongly dependent on the moisture barrier formed by the coatings, the permeability has to be characterised too. Literature is available for the permeability of coatings in different application areas such as food technology [7], building materials [10], violin varnishes [8], canvas paintings [11] and panel paintings [4, 6, 9]. The focus of [4] is again on ageing. In [6, 9], the permeability of ground layers, paint layers and varnishes is investigated by cup tests driven for composites of wood with partial or full stratigraphy. In the contribution at hand, the permeability of the coatings is examined by the cup method using highly permeable polyethylene (PE) frits as support material. In this manner, the coatings are tested individually in order to be able to predict the permeability of different coating systems. Since the combination of permeability values obtained by single tests might not be reliable, which is also discussed in [9], tests of total and partial coating systems are carried out on PE frits.

The selection of investigated coatings is based on three artworks that are currently under investigation at the Institute for Structural Analysis of Technische Universität Dresden (ISD) together with the University of Fine Arts Dresden (HfBK). A painted cupboard from the eighteenth century as a sample of furniture from Upper Lusatia and a panel painting by L. Cranach the Elder ("Katharinenaltar", left wing, inner side), exhibited in the Dresden State Art Collections (SKD) are investigated within the project *CultWood* (see funding statement). Both artworks or classes of artwork have been objects of research in the past with an art technological focus [14–18] as well as with a numerical focus [19]. The Russian icon ("Last supper") from 1912 is investigated within the project *VirtEx* (see funding statement). Also, this class of objects has been the object of technological [20–23] and numerical [24] research.

Materials and methods

Two different series of coating systems are investigated which are based on the coatings of three original objects: the cupboard from the eighteenth century and the altarpiece by L. Cranach the Elder from the sixteenth century (subsequently named C-series) and the Russian icon painting from the beginning of the twentieth century (subsequently named I-series). The division into two series is based on different applied test procedures. For the C-series, the focus is on permeability tests of single coatings, while for the I-series the focus is on permeability tests of composed coating systems.

For both series, permeability tests with the cup test method are carried out. Furthermore, the specimens from the I-series are tested mechanically by tension tests. This section subsequently describes the materials and production technology of the test specimens in "Materials" section and "Specimen preparation" section, and the experimental and analytical methods in "Methods" section.

Materials

The investigated coatings are listed in Table 1. The coatings based on the Cranach panel painting and on the Upper Lusatian cupboard are assigned to the C-series, while the coatings based on the Russian icon are assigned to the I-series. Also, the components and applying modes are given in Table 1. A further description is documented in the following sections.

Materials for the C-series

Pre-sizing A rabbit skin glue is used for the C-series (supplier Kremer Pigments) with the following technical properties: Bloom value 340 g–360 g, pH value of 6.0–7.5, viscosity of 4.25–5.50°E (degree Engler for 17.75% and 60 °C) and a fat content of 1.0–2.5% (manufacturer information). Less content of fat provides a more elastic character of the material, but entails a low binding power.

White ground The chalk of the ground layer of the C-series is acquired from Champagne (Kremer Pigments).

Egg tempera (C) For the C-series, an egg tempera is prepared which consists of egg yolk (without membrane) from eggs of a domestic chicken which is diluted by pure linseed oil (Kremer Pigments). The colorant of the C-series is Terra di Sienna, an earth pigment (Kremer Pigments). The volume proportions of egg yolk, linseed oil and pigments are 5:3:1.

Distemper The distemper of the C-series consists of rabbit skin glue and a colourant in a weight ratio of 2:1. The colourant for the distemper of the C-series is Verona green earth (Kremer Pigments).

Resin oil colour The oil colour of the C-series is a mixture of pure linseed oil, pine turpentine, Venetian turpentine and light ochre (Kremer Pigments). The volume ratio of pine turpentine and Venetian turpentine is 3:1, the volume ratio of light ochre and linseed oil is 2:1.

Table 1 Coatings for the mechanical tests and permeability test: recipes with the components, application modes and series assignment

Coating	Series	Recipe	Application
White ground	C	7% chalk from Champagne	1 × dabbed, 2 × painted (crosswise)
Isolation	C	3.5% rabbit skin glue in aqua dest	1 × painted
White imprimatura	C	1 VF[1] linseed stand oil + 2 VF lead white (ground with a slab)	1 × painted
Resin oil varnish (Mechelner[2])	C	Straßburger Turpentine (170.75 g) + linseed stand oil (170.75 g) + lead red (170.75 g) + pine turpentine (600 ml)	1 × painted
Linseedoil varnish	C	linseed oil, siccativated with manganese	1 × painted
Resin oil colour ([25], p. 645, receipe 2)	C	1 VF paintmedium (1 VF Venetian Turpentine + 3 VF pine turpentine) + 1 VF oil colour (1 VF linseed stand oil + 2 VF light ochre)	1 × painted
Egg tempera (C)	C	1VF Terra di Sienna (281 g) + 5 VF egg yolk without membrane (518 g) + 3 VF linseed oil (316 g) total 1115 g tempera	1 × painted
Distemper	C	7% rabbit skin glue (667 ml) in aqua dest. + Verona green earth (333 g)	1 × painted
Beeswax		2 VF pine turpentine + 1 VF beeswax	
Sizing + textile	I	pre-sizing of 12% uncleaned hide glue, 28% glue solution embedding the textile	1 × painted, 2 × painted embedding the textile
Hardwhite	I	55.6 g water + 4.1 g glue + 56 g chalk for 1 layer	1 × dapped
Primer	I	40.9 g water + 3.08 g rabbit skin glue + 56 g chalk	6 × painted
Egg tempera (I)	I	35% pigment, 8.5% binding medium, 56.5% water	3 × painted
Olifa	I	80% linseed oil and 20% commercial hard drying	1 × painted, excess removed
Spirit varnish	I	25% dammar, 25% Shellsol A, 50% white spirit	1 × painted

[1] VF: volume fraction, [2] varnish Mechelner describes a varnish of a historical recipe [26]

Imprimatura The binding medium for the white imprimatura layer of the C-series is linseed stand oil (Kremer Pigments), a specially prepared linseed oil for coatings. The oil is heated without oxygen, which increases the viscosity and its drying time is slowed resulting in better ageing properties. The linseed oil is mixed with lead white pigments with a volume ratio of 1:2 (linseed oil per lead white).

Linseedoil varnish For the first varnish of the C-series, a pure linseed oil siccativated with manganese is used (both Kremer Pigments).

Resin oil varnish The so-called Mechelner varnish is based on a historic recipe (see [26], p. 619). It consists of Strasburger turpentine, linseed stand oil, lead red pigment and pine turpentine (all Kremer Pigments). Strasburger turpentine describes a special historic turpentine, consisting of high qualitative larch turpentine. The used pigments are lead white, lead red, iron oxide red, light ochre (all Kremer Pigments).

Beeswax This coating is not part of the coating system of the panel painting of Cranach or of the Lusatian cupboard. However, it is tested additionally for the C-series, since it is often used for the sealing of wooden artwork. The coating is a mixture of balsamic turpentine oil and beeswax (Kremer Pigments 62,200) with a volume ratio of 2:1. The materials are heated until the wax is melted. A milky cloudy paste is formed.

Materials for the I-series

Sizing and textile For the pre-sizing and sizing layers, two kinds of collagen based glue are used. The first one is a traditional uncleaned hideglue from stock of the conservation department of the Saxon State Office for Cultural Heritage (Landesamt für Denkmalpflege, see [27]). This traditionally uncleaned hide glue has an estimated Bloom value of 200 g. The second kind of glue that is used is a rabbit skin glue with a Bloom value of 400 g by Eytzinger (Schwabach, Germany). The pre-sizing consists of a 12% solution of uncleaned hide glue, and the sizing is a solution of 25% uncleaned hide glue, 3.5% rabbit skin glue and 71.5% water.

The textile of the I-series is a cotton tissue, called cheesecloth (Provider Eagle Home Products Inc., Huntington NY, USA), of a thread count of 4 lateral and 8 longitudinal threads per centimeter and a grammage of 37 g/m^2 (own measurement).

Hardwhite and primer The chalk of the I-series is a finely ground chalk from Champagne region consisting of 99.7% calcium carbonate (supplier Eytzinger, Schwabach, Germany). The binding medium for both primer layer and hardwhite is the above mentioned rabbit skin glue. The primer is produced using traditional recipes. The proportions by weight are 44% glue solution and 56% chalk. After drying, the primer layer consists of 94.8% chalk and 5.2% rabbit skin glue. To prepare the hardwhite, an amount of 16 g of rabbit skin glue solution (7% in water) is added to 100 g of prepared primer. The recipe of hardwhite could then be described as 55.8 g water + 4.2 g glue + 56 g chalk. After drying, the hardwhite layer consists of 93.0% chalk and 7.0% glue. The production is described in detail in [29], p. 385.

Egg tempera (I) The binding medium for the paint layer of the I-series is egg yolk from domestic chickens. Dry white wine (Pinot Gris from Saale-Unstrut region) is used as a diluent and additive. To make the emulsion (tempera binder), one part by volume of egg yolk is mixed with four parts dry white wine. To mix the pigment with the emulsion, the pigment and the emulsion are ground with a slab. The paint consists of 35% pigment, 8.5% binding medium and 56.5% water. The pigments for the paint layer of the I-series are Siena nature (supplier Kremer Pigments, item No. 40400) for the specimen No. 46–57 (see Table 2). For the specimens of the I-series No. 58 – 67 and the tensile test specimens, a mixture of natural iron oxide pigments, Harzocker (Kremer Pigments, item No. 40360) and Terra Pozuoli (Kremer Pigments, item No. 40440) is applied.

Olifa For the olifa of the I-series, a mixture of fresh linseed oil (80%) and a commercial hard-drying oil (20%, supplier Kremer Pigments, item No. 79021) are used. The hard-drying oil is used to adjust the drying time. It contains linseed oil, colophonium and drying agents.

Table 2 Cup test specimens, specimen numbers and associated coatings

specimen name	specimen No.	white ground	white imprimatura	resin oil varnish	linseedoil varnish	resin oil colour	egg tempera (C)	distemper	beeswax
C_{wg}	1-5	x							
C_{wi}	6-10	x	x						
C_{rv}	11-15	x		x					
C_{lv}	16-20	x			x				
C_{rc}	21-25	x				x			
C_{et}	26-30	x					x		
C_{di}	31-35	x						x	
C_{bw}	36-40	x							x
C_{tot}	41-45	x	x	x		x	x		

specimen name	specimen No.	sizing + textile	hardwhite	primer	egg tempera (I)	olifa	spirit varnish
I_1	46-49	x					
I_2	50-51	x	x				
I_3	52-53	x	x	x			
I_4	54-57	x	x	x	x	x	
I_{tot}	58-67	x	x	x	x	x	x

Varnish For the spirit varnish of the I-series, one part by weight of gum dammar (Kremer Pigments, item No. 60000) dissolved in two parts white spirit (boiling range 100 – 140 °C, Kremer Pigments, item No. 70400) and one part of Shellsol A (mixture of aromatic hydrocarbons, boiling range 165 – 180 °C, Kremer Pigments, item No. 70520) are used.

Supporting material for the permeability test

To measure the water vapour permeability, the investigated coatings are applied on polyethylene (PE) frits since the coatings are not able to build self-sustaining films. For this purpose, filter disks of the producer *KIK Kunststofftechnik* are used. According to the producer, the PE frits have a homogeneous porous structure, a relatively high water vapour transmission rate and a high resistance towards any kind of liquids. Due to the known constant and homogeneous properties of the PE frits, it is easy to recalculate the permeability of the coatings from the permeability of the frit-coating-composite. The manufacturer's data of the PE frits are shown in Table 3.

Table 3 Properties of the supporting PE frits for the investigation of the water vapour permeability of the coatings

Property	Unit	Value
Diameter	mm	107.2
Thickness	mm	6.0–6.2
Raw density	g/mm^3	0.6
Tensile strength	N/mm^2	5
Mean pore diameter	µm	40
Pore volume	%	45

Specimen preparation

Permeability test specimens for the C-series

For the C-series, the specimens are schematically shown in Fig. 1, the association of coatings to the specimens can be found in Table 2. The following coating procedure is applied for the total coating system (C_{tot}). The first layer is the pre-sizing, which is followed by white ground, which is dabbed one time and painted two times crosswise. This ground is isolated by a thin layer of rabbit skin glue coating. After that, the first layer of paint bounded with egg tempera is applied. The imprimatura is applied after the egg tempera layer. After that, the second paint layer, the resin oil colour, follows. Finally, the varnish is applied with a varnish brush. In case of beeswax coating, the material is rubbed in with a linen cloth.

For the determination of the diffusion properties of every single paint layer, the layers are applied separately to sintered porous polyethylene frits (PE frits). Due to the porosity of the frits and the resulting penetration of the binder medium, the paint layers do not form a homogeneously closed film. For this reason, all frits are primed with a white ground layer, on which the other layers of paint are applied afterwards. A selection of coated frits can be seen in Fig. 2. The age of the coatings at the time of testing is given in Table 4.

Permeability test specimens for the I-series

The coating system consists of different layers (see Fig. 3): pre-sizing, sizing with textile, first layer of ground (hard-white), actual ground layer (primer), paint layer (egg tempera), olifa that penetrates the paint layer and upper parts of the ground, and a spirit-varnish. A detailed description of the manufacturing of this coating system is given in [29]. The main facts are described in the following.

Sizing and textile The first layer has to be a traditional thin pre-sizing to avoid an uncontrolled adsorption of

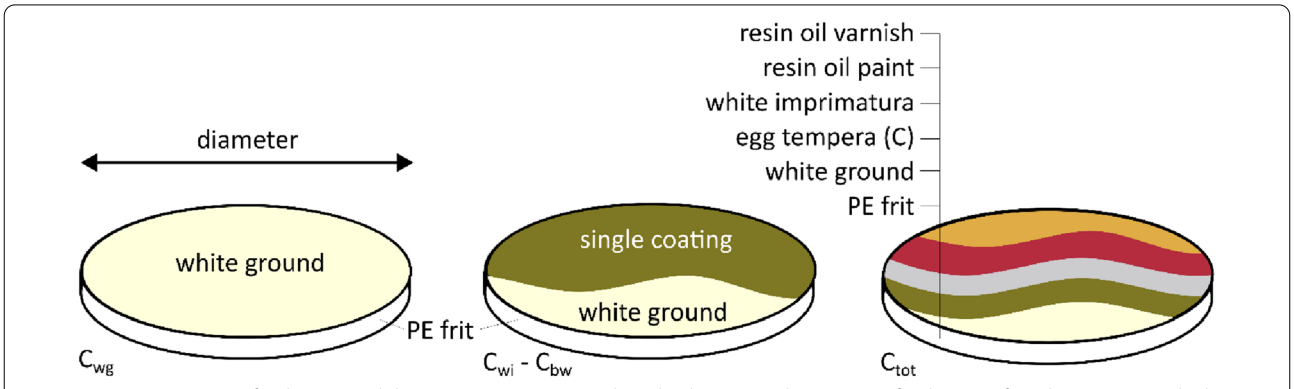

Fig. 1 C-series: specimens for the permeability test, one specimen only with white ground, specimens for the test of single coatings applied on white ground and one specimen with a full coating system of a painting

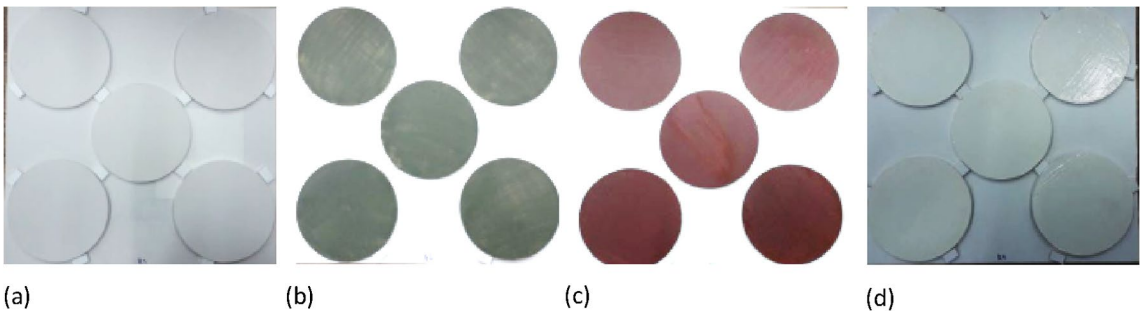

Fig. 2 Specimens of painted test-frits: (**a**) white ground with collagen based glue isolation for every experiment and the following coating systems, (**b**) distemper on white ground, (**c**) egg tempera on white ground, (**d**) varnish on white ground

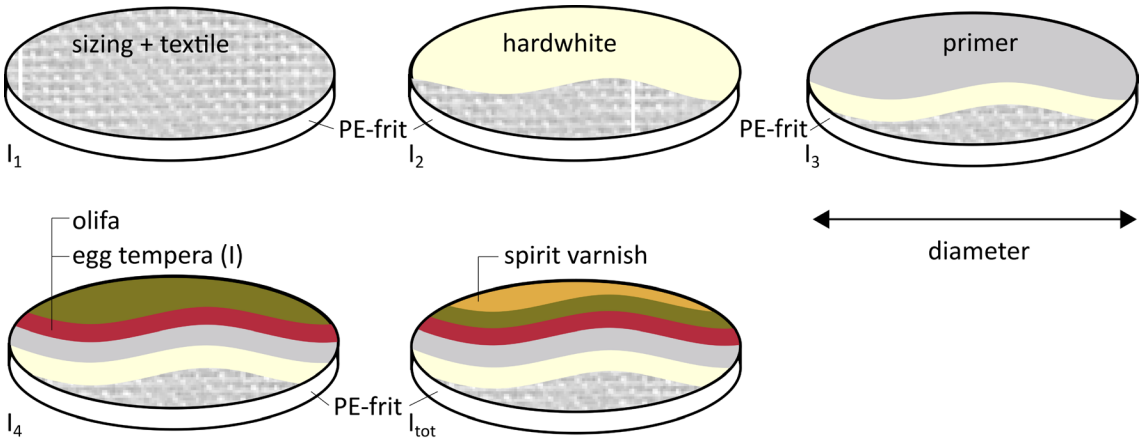

Fig. 3 I-series: specimens for the permeability test using a consecutive testing strategy, five specimens with different number of coatings

the thick glue layer by the untreated specimen. A thin wash of a 12% solution of 55 °C warm uncleaned hide glue is applied on the PE frit, approx. 0.02 – 0.04 g/frit (0.00022 – 0.00044 g/cm^2).

To create the thick layer of sizing, similar to that present on the icon (see [29]), a solution of 25% uncleaned hide glue, 3.5% rabbit skin glue and 71.5% water is applied onto the PE frit. The results of pre-tests show that to reach a layer of 0.2 mm pure hide glue, it is necessary to apply 0.07 g/cm^2 (6.3 g/frit). This solution must not be too warm to allow for it to gel right after application. To obtain a more even layer, the about 30 °C warm solution is brushed on in two steps. The textile is laid on the first layer of gelled glue right before the next layer of solution is applied.

Hardwhite and primer The ground layer consists of two different components: hardwhite and actual primer. As the hardwhite is being prepared, it is heated to 50 °C and dapped into the freshly applied sizing layer. Then, the still warm hardwhite-primer is mixed with the gelled sizing. As a result, the connection of the primer layers to the sizing is thought to be improved.

This layer is followed by six layers of the basic chalk-glue-primer. They are painted by using soft brushes. The surface is allowed to dry after each layer. It turned out that it is difficult to apply the primer layers without small bubbles appearing ("needle pin holes"). These holes affect the water vapour permeability. In areas, where too many of them appeared, the dried surface is rubbed with a damp cloth to close the holes before the next chalk ground layer is applied. The thickness of the ground layer is checked using a scalpel. If the goal thickness of 0.7 – 1 mm is not reached, another one or two layers are applied.

After drying completely, the surface is smoothed with sandpaper (grain 240) and with a damp cloth. The specimens show significant cupping due to the shrinkage of the sizing and ground layers.

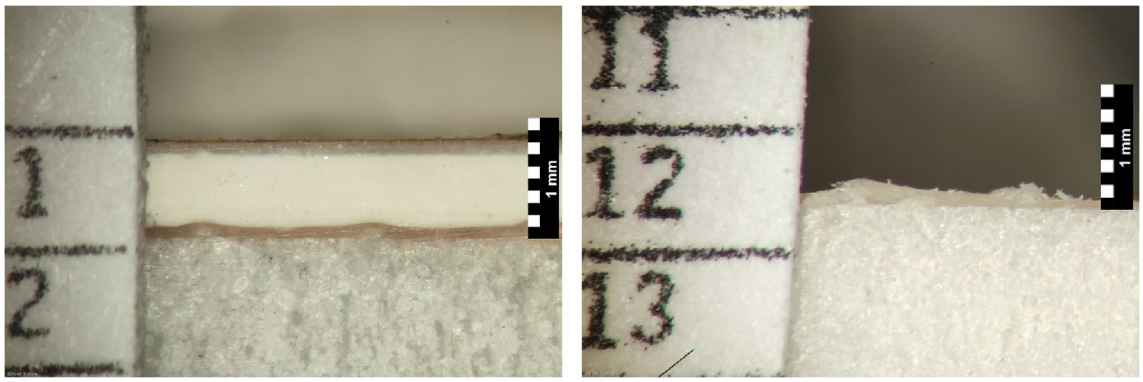

Fig. 4 Microscope images of the thickness measurement of two coatings of the I-series: (**a**) I_{tot} specimen No. 54 with total coating system and (**b**) I_1 specimen No. 49 with sizing and textile layer (cf. Table 2)

Egg tempera (I) The paint is applied in three thin layers using a very soft brush, allowing each layer to dry. The average thickness of the complete paint layer proved to be 30 – 40 µm, like most of the paint layers on the original icon. The layer thickness is measured by microscope images, see Fig. 4.

Olifa The olifa is applied with a soft brush. An average amount of 0.5 g/frit is used. Right before the final drying of the oil film, excess oil is removed from the surface with the heel of the hand. The amount of oil removed is weighed and subtracted from the amount of oil originally applied. The olifa mass varies from 0.4 – 0.58 g/frit with two outliers (I-series No. 58: 0.32 g/frit and No. 67: 0.68 g/frit).

Spirit varnish After drying for two weeks, the layer of dammar varnish is applied. It is brushed on very quickly to avoid dissolving the olifa. The weight of the dried varnish is approximately 0.06 g/frit.

Mechanical test specimens for the I-series

The mechanical behaviour is investigated for the total coating system of the I-series, based on the coating system of the Russian icon. The coatings are applied on the textile embedded in the sizing without any supporting material to test the mechanical properties of the coating system only. Additionally, tests are conducted for the sizing and textile without further coatings. For each specimen type, 10 specimens are tested. The specimens are schematically shown in Fig. 5.The width *w* and thickness *t* of the specimens can be found in Table 5.

Methods

Mechanical test method

The stress–strain relations are tested for a partial coating system $I_{1,t}$ consisting of the sizing and textile layers (S + T) of the Russian icon specimens of the I-series and for the total coating system $I_{tot,t}$, i.e. the composite of all coating layers on top of the (wooden) support. Tension tests are conducted at 65% relative humidity (*RH*). This composite is rather exceptional with a thick collagen based glue layer (S + T) of ca. 0.33 mm on average for $I_{1,t}$, primer, paint and varnish with a total thickness of ca. 1.30 mm on average for $I_{tot,t}$ (see "Permeability test specimens for the I-series" Section).

The experimental mechanical tests are performed after 30 days of drying in a standard European room climate after the last production step on a Universal Testing Machine (Hegewald&Peschke, Inspect10) equipped

Table 4 Cup test climates of the test specimens at constant temperature T = 23°C

Cup test climates (inside/outside)	RH 0% / 50%	RH 0% / 85%	RH 85% / 50%	RH 95% / 50%
C-series	x	x		x
Drying time	3 months	4 months		6 months
I-series	x		x	x
Drying time I_1-I_4 Drying time I_{tot}	3 months 6 months		6 months	6 months

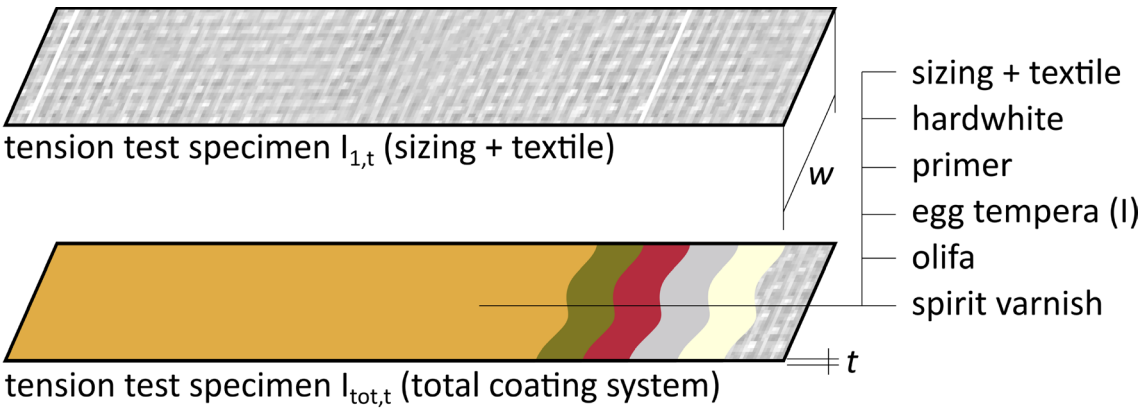

Fig. 5 Tension test specimens of the I-series of $I_{1,t}$ and $I_{tot,t}$ specimens with the sizing and textile and the total coating system of the Russian icon, respectively

with a 10 kN load cell. An initial force of 5 N is set as the starting point of the measurements. The tests are conducted in a displacement-controlled mode at a rate of 1.5 mm min^{-1} for the more ductile $I_{1,t}$ specimens (S + T) and of 0.3 mm min^{-1} for the more brittle $I_{tot,t}$ specimens (total coating system). 10 successful tests are obtained for each configuration.

Brittle failure is expected, where the maximum stresses are followed by immediate failure. Thus, the tension strength f is directly taken as the maximum, ultimate stress σ_u. The Young's modulus E is determined in the range between 10 and 40% of the ultimate stress as stated in EN-408 [28].

Furthermore, a simple isotropic strain-dependent damage material model for this coating system is derived [30]. Therein, the initial stiffness E becomes the reduced stiffness E^* by way of a damage variable d

$$E^* = (1 - d)E \tag{1}$$

where the damage variable is dependent on the history variable κ with $d = d(\kappa)$ as

$$d = \begin{cases} 0, & \kappa \leq \kappa_0 \\ \frac{1}{2}\left(1 - \cos\left(\frac{\kappa - \kappa_0}{\kappa_{cr} - \kappa_0}\pi\right)\right), & \kappa_0 \leq \kappa < \kappa_{cr} \\ 1, & \kappa > \kappa_{cr} \end{cases} \tag{2}$$

The internal history variable κ is described as a multiple of the ultimate strain, where $\kappa = \kappa_0$ initialises the reduction of stiffness and $\kappa = \kappa_{cr}$ terminates the damage growth, leading to a stiffness equal to zero. Detailed information on the concept of damage modelling are published in e.g. [30]. In the results section, the damage model parameters are fitted to the experimental results.

Permeability test method

For all coating materials of the C- and I-series, the permeability is tested using the cup method. The procedure of the diffusion test called the *cup method* is described in DIN EN ISO 12572 [31] in combination with DIN EN ISO 7783 [32]. PE frits, which have a high water vapour permeability, are used as carrier material, see "Supporting material for the permeability test" Section. Two different strategies are used: For the C-series, the coatings are tested individually on a PE frit with white ground. White ground is necessary, because the other coatings either do not form a closed film on the PE frit or penetrate the pores. Additionally, a total coating system is tested for comparison. For the I-series, the coating system is tested consecutively adding one coating for the next specimen type.

After coating the PE frits and allowing the coatings to dry, the side faces of the frits are sealed to ensure one-dimensional water vapour diffusion. The frits are fixed on a glass cup which is filled with salts or oxides (standardised in [31]) for the dry cup tests and with an ammonium dihydrogen phosphate solution for 95% or potassium chloride for 85% relative humidity inside the cup for the wet cup test. In the steady state wet and dry cup test, one obtains the density of water vapour flow rate g. By the density of water vapour flow rate and the water vapour pressure difference Δp_v, the water vapour resistance

$$Z = \frac{\Delta p_v}{g} \tag{3}$$

of the PE frit-coating-composite is calculated. A correlated quantity is the permeance

$$W = \frac{1}{Z} \tag{4}$$

This property changes for the same material with different coating thicknesses. Therefore, the permeability

$$\delta = t \cdot W = \frac{t}{Z} \tag{5}$$

is used as a material parameter, which is independent of the coating's thickness t. The total water vapour resistance of composites is calculated additively

$$Z_{tot} = \frac{1}{W_{tot}} = \sum\nolimits_c \frac{1}{W_c} = \sum\nolimits_c \frac{t_c}{\delta_c}, \tag{6}$$

where the index c denotes the properties of a single coating and *tot* denotes the properties of the total coating system. The resistance of the PE frit, which is known beforehand, is subtracted to obtain the coating system properties. The same method is used for the parameter determination of the added layer in the consecutive testing strategy.

Since the permeability properties of the coatings are expected to be dependent on the relative humidity at the coating, several tests are conducted using the dry cup and wet cup tests. Three different climates are tested for each coating system (see Table 4). The temperature is kept constant at 23 °C for all tests. The inside relative humidity is controlled by salts, oxides and aqueous solutions, the outside relative humidity by a climate chamber.

By the water vapour resistance of the PE frit and the different layers, the water vapour profile can be calculated for each test by Eqs. (3) and (6). This allows to find the average water vapour pressure or relative humidity in the investigated coatings during the tests.

The permeability δ is chosen as a material parameter because it characterises the coating's material properties independently of the thickness of the coatings. The RH-dependent permeability can be described by an exponential function, which is an established approach to describe the diffusion in hygroscopic materials, e.g. [33, 34] and, thus, is adapted here for the permeability. The advantage of this approach is that the permeability is not negative for the whole range from 0%RH to 100%RH when using an exponential equation. After all, a negative permeability value would be unphysical. The function

$$\delta_c = a_c \cdot e^{b_c \cdot RH_c} \tag{7}$$

contains the model parameter a_c, representing the permeability of the dry coating, and b_c, representing the dependency of the permeability on the relative humidity. Although RH is not a material parameter of the coating, in contrast to the moisture content as a weight fraction of the materials mass, it describes the dependency in a phenomenological but simple manner. This seems to be reasonable, because not all coatings are hygroscopic and, therefore, the driving potential is the water vapour pressure gradient, which is related to RH. It should be noted that the model extrapolates the material properties for RH-values outside the range of the minimum and maximum of tested conditions and are less trustworthy, especially for high RH values.

Results and discussions

Mechanical test results

Some of the tested broken specimens are shown in Fig. 6. Figure 7 depicts the experimental results of force–displacement and stress–strain characteristics of the investigated specimens. Since the sizing and textile layers of specimens $I_{1,t}$ are relatively thin, the maximum force is lower than those of the total coating system of specimens $I_{tot,t}$, where the ultimate force is larger, especially with respect to the massive ground layer.

The strength of the total coating system of $I_{tot,t}$ is nearly the same as the strength of the sole sizing and textile layer of $I_{1,t}$. On the other hand, $I_{tot,t}$ is much stiffer than

Table 5 Tension test of $I_{1,t}$ (sizing and textile) and $I_{tot,t}$ (total coating system) (RH/T = 65%/20°C): mechanical and geometrical characteristics (statistical estimators)

Layers	Statistical estimator	Strength $f\left[\frac{n}{mm^2}\right]$	Ultimate strain $\varepsilon_u[10^{-3}]$	Young's modulus $E\left[\frac{n}{mm^2}\right]$	Thickness t[mm]	Width w[mm]
$I_{1,t}$ (sizing and textile)	Median	9.86	8.96	1370	0.32	20.40
	Range	[8.30…13.24]	[6.25…12.50]	[842.7…1883]	[0.30…0.38]	[20.04…20.68]
	Mean value	10.34	9.01	1320	0.33	20.38
	Standard deviation	1.64	2.11	300.0	0.027	0.24
$I_{tot,t}$ (total coating system)	Median	9.69	4.88	4914	1.25	20.78
	Range	[6.47…11.78]	[1.08…5.83]	[3181…31117]	[1.10…1.50]	[19.95…21.00]
	Mean value	9.75	3.98	-	1.30	20.64
	Standard deviation	1.48	1.75	-	0.160	0.35

Fig. 6 I-series: broken $I_{tot,t}$ specimens of the total coating system after the tension tests

$I_{1,t}$, which can also be seen in the boxplot in Fig. 7c. It has to be emphasized again that these experiments only describe the conditions of a one month old and intact coating system tested in one constant climate. For these conditions, the sizing and textile layers do not seem to give any mechanical improvement to the total coating system, except for a contribution to the overall thickness and, thus, a slightly larger maximum force. The larger ductility may be an advantage to ensure a solid bond also for aged or damaged upper coating layers, i.e. when they get more brittle or cracked. Besides, it has a high water vapour resistance, which reduces swelling and shrinkage of the wooden support and consequential stresses in the coating system when the upper coating layers are damaged.

Statistical estimators of all test results are listed additionally in Table 5. It has to be emphasized that for some characteristics, the standard normal distribution is not meaningful for a given quality of data, see e.g. [35]. The Young's modulus data of the total coating system of $I_{tot,t}$, for example, show two outliers which, according to the knowledge of the authors, cannot be ascribed to experimental or modelling errors and, thus, are not excluded. For that reason, Table 5 and Figs. 7b and c give several result quantifications and statistical estimators of the mechanical characteristics.

The modelled damage behaviour by the degradation of the Young's modulus is visualised in Fig. 7d together with the experimental test results of the total coating system. The parameters of the damage function are listed in Table 6. With respect to the quality of the experimental data, the median values are chosen as the basis for the parameter identification (cf. Figure 7b). Due to the phenomenological approach, the model parameters do not describe the physical ultimate strain at the same point of the ultimate stress. It is the configuration fitting the experimental results best for this numerically stable approach.

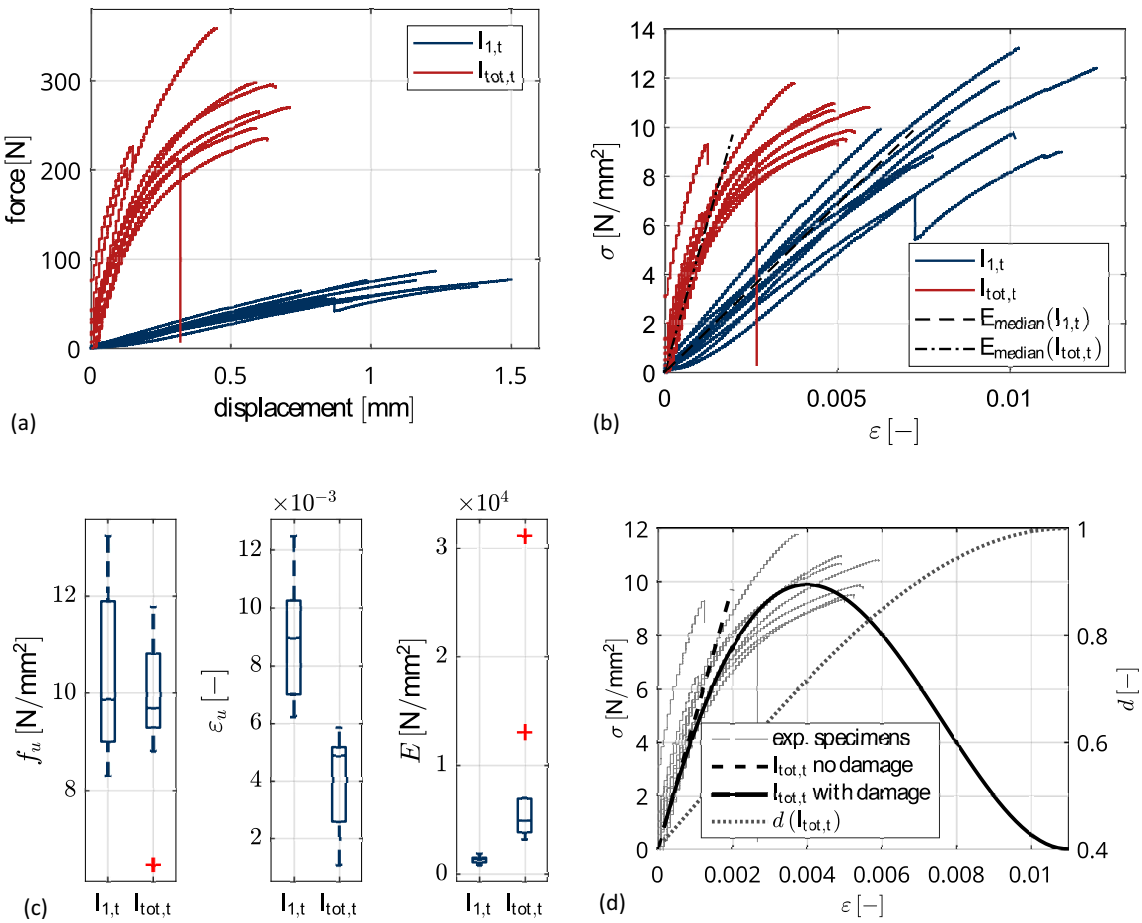

Fig. 7 Tension test of $l_{1,t}$ (sizing and textile) and ltot,t (total coating system) (RH/T = 65%/20°C): (**a**) force–displacement and (**b**) stress–strain relations, (**c**) boxplot of the mechanical characteristics, (**d**) stress–strain relations of experiments and model of total coating system, with and without consideration of damage

Table 6 Parameters of the damage function of the coating system

Parameter	Quantity
$E\left[\frac{n}{mm^2}\right]$	4914
$\varepsilon_u[-]$	$4.875 \cdot 10^{-3}$
$\kappa_0[-]$	$-1.75 \cdot \varepsilon_u$
$\kappa_{cr}[-]$	$2.25 \cdot \varepsilon_u$

Results of the permeability tests

Permeability of the C-series coatings

For every type of the coatings of the C-series, the average thicknesses of the coating layers are determined by a microscope at two specimens per type. At each observed specimen, the thickness is measured at ten points distributed over the coated area, to obtain representative values. The mean value of all measurements per coating is taken for Eq. (5) and is given in Table 7 for the investigated coatings of C_{wi} to C_{bw}. The values of all coatings of the coating

Table 7 Mean value and standard deviation of the measured thicknesses of the single coating specimens C_{wi}—C_{bw}

Coating	White ground	White imprimatura	Resin oil varnish	Linseedoil varnish	Resin oil colour	Egg tempera (c)	Size colour	Beeswax
Thickness [µm]	248 ± 124	35 ± 8	17 ± 6	17 ± 5	96 ± 21	77 ± 6	76 ± 20	11 ± 4

Table 8 Mean value and standard deviation of the measured thicknesses of all coatings of the total coating system of the C-series, C_{tot}, specimens No. 41, 44 and 45

Coating	White ground	Egg tempera	White imprimatura	Oil colour	Resin oil varnish
Thickness [µm]	404 ± 89	87 ± 7	53 ± 1	36 ± 3	34 ± 23

system of C_{tot}, used in Eq. (6) are given in Table 8. In Fig. 8, two of the microscope images can be seen.

The permeability of each coating is calculated from the measured densities of water vapour flow (see Table 9) as well as the associated relative humidity, determined by the calculation of the humidity profile, and can be found in Table 10 for the C-series. Different relative humidity values are found in the coatings even for the same experimental setup because the permeability influences the moisture gradient in the specimen.

For the specimens of type C_{di}, the frits coated with white ground and distemper, the water vapour resistance calculated from the water vapour flow is in the order of magnitude of that of the C_{wg} specimens (white ground). Thus, the water vapour resistance of distemper is negligibly small and is therefore not considered further.

The permeability of the other coatings of the C-series are shown in Fig. 9. It can be seen that the permeability of all coatings is larger for larger relative humidity. The largest values of permeability is present for the specimens of white ground and egg tempera. The largest water vapour resistance are shown in the specimens of beeswax and resin oil varnish.

Exponential regression functions are added to Fig. 9. By the regression functions, it is easy to compare both the water vapour permeability as well as the degree of humidity dependency. The humidity dependency can be read from the curvature of the regression functions or from the rise of the regression functions in the logarithmic plot.

In Fig. 10, the parameters a_c and b_c of the exponential function in Eq. (7) are shown and compared for all coatings of the C-series. The parameter a_c is a measure of the permeability of dry coatings. The most permeable material, white ground, shows by far the largest value of a_c, while beeswax has a negligibly small parameter a_c. The parameter b_c is a measure of the humidity dependency. The largest humidity dependency is present for beeswax, while the varnishes exhibit a low dependency. Finally, the parameters a_c and b_c are given in Table 11. It has to be noted that the exponential function leads to very high values of permeability for high *RH* values. Due to the extrapolation, it is not

Table 9 Measured stationary density of water vapour flow g through the coated and uncoated PE frits for the three cup test settings of the C-series

RH 0%/50%			RH 0%/85%			RH 95%/50%			RH 95%/50%		
specimen		$g\left[\frac{g}{m^2 \cdot d}\right]$	specimen		$g\left[\frac{g}{m^2 \cdot d}\right]$	specimen		$g\left[\frac{g}{m^2 \cdot d}\right]$	specimen		$g\left[\frac{g}{m^2 \cdot d}\right]$
C_{wg}	4	201.1	C_{wg}	4	590.0	C_{wg}	1	291.0	C_{et}	26	209.0
	5	200.3		5	588.6		2	325.0		27	191.0
C_{wi}	9	55.3	C_{wi}	9	138.1		3	296.0		28	192.0
	10	65.7		10	161.4	C_{wi}	6	77.0	C_{di}	31	325.0
C_{rv}	14	21.6	C_{rv}	14	45.0		7	93.0		32	328.0
	15	25.9		15	96.4		8	90.0		33	304.0
C_{lv}	19	124.0	C_{lv}	19	302.2	C_{rv}	11	28.0	C_{bw}	36	2.7
	20	112.2		20	313.7		12	39.0		37	3.6
C_{rc}	24	9.4	C_{rc}	24	47.3		13	30.0		38	4.9
	25	7.3		25	19.9	C_{lv}	16	160.0	C_{tot}	41	6.2
C_{et}	29	118.6	C_{et}	29	355.4		17	159.0		44	5.4
	30	112.4		30	346.5		18	164.0		45	6.5
C_{di}	34	209.3	C_{di}	34	552.2	C_{rc}	21	19.4	PE	ref.	495.0
	35	203.3		35	559.0		22	27.5			
C_{bw}	39	3.0	C_{bw}	39	10.0		23	22.1			
	40	2.5		40	32.2						
PE	ref.[1]	404.0	PE	ref	760.0						

[1] ref.: reference value for the evaluation, no specimen number

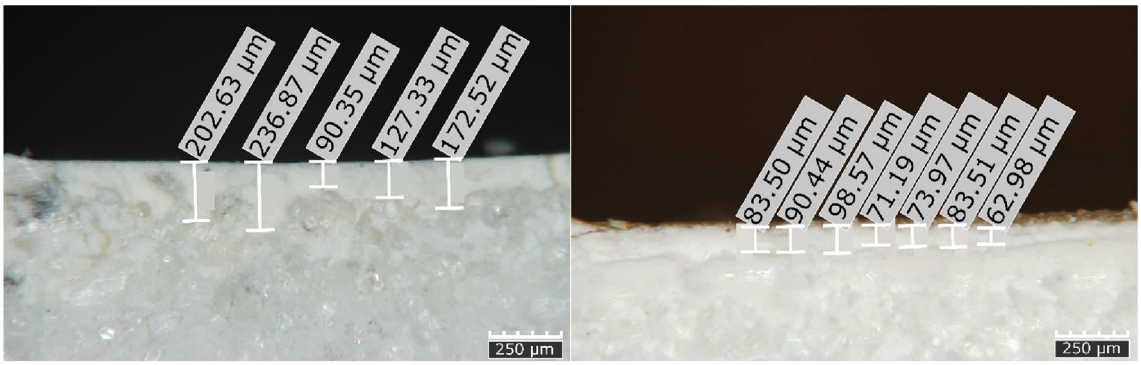

Fig. 8 Microscope images for the thickness measurement of white ground: (**a**) specimen C_{tot} (specimen No. 5) and (**b**) specimen C_{wi} (specimen No. 6)

certain whether this reflects the actual material behaviour. For white ground, the largest extrapolated value is 28 times *a*, while the largest measured value is 12 times *a*. However, this issue is not relevant, since white ground has a relatively high permeability and the resistance of coating systems is dominated by the coatings with the largest resistance values. This issue is more important for beeswax, where the largest extrapolated value is 200 times *a*, while the largest measured value is 18 times *a*. Therefore, the authors recommend further investigations of the permeability of beeswax for high *RH* values.

Table 10 Permeability and associated relative humidity of the coatings from the C-series calculated from measured g

Coating	RH 0% / 50%		RH 0% / 85%		RH 95% / 50%	
	***RH*[%]**	$\delta\left[\frac{kg \cdot m}{Pa \cdot m^2 \cdot s}\right]$	***RH*[%]**	$\delta\left[\frac{kg \cdot m}{Pa \cdot m^2 \cdot s}\right]$	***RH*[%]**	$\delta\left[\frac{kg \cdot m}{Pa \cdot m^2 \cdot s}\right]$
White ground	37.44	$8.17 \cdot 10^{-13}$	75.49	$3.17 \cdot 10^{-12}$	59.27	$1.60 \cdot 10^{-12}$
	37.39	$8.11 \cdot 10^{-13}$	75.42	$3.13 \cdot 10^{-12}$	57.73	$2.15 \cdot 10^{-12}$
					59.05	$1.67 \cdot 10^{-12}$
White imprimatura	30.71	$2.04 \cdot 10^{-14}$	51.70	$2.96 \cdot 10^{-14}$	67.57	$3.12 \cdot 10^{-14}$
	31.78	$2.57 \cdot 10^{-14}$	53.25	$3.62 \cdot 10^{-14}$	66.54	$4.01 \cdot 10^{-14}$
					66.73	$3.83 \cdot 10^{-14}$
Resin oil varnish	27.47	$3.32 \cdot 10^{-15}$	45.63	$3.95 \cdot 10^{-15}$	70.56	$4.71 \cdot 10^{-15}$
	27.97	$4.07 \cdot 10^{-15}$	49.20	$9.31 \cdot 10^{-15}$	69.80	$6.81 \cdot 10^{-15}$
					70.42	$5.08 \cdot 10^{-15}$
Linseedoil varnish	40.51	$4.56 \cdot 10^{-14}$	64.34	$5.10 \cdot 10^{-14}$	60.67	$5.23 \cdot 10^{-14}$
	39.04	$3.57 \cdot 10^{-14}$	65.17	$5.52 \cdot 10^{-14}$	60.74	$5.16 \cdot 10^{-14}$
					60.37	$5.52 \cdot 10^{-14}$
Resin oil colour	26.11	$7.80 \cdot 10^{-15}$	45.84	$2.40 \cdot 10^{-14}$	71.12	$1.82 \cdot 10^{-14}$
	25.86	$6.00 \cdot 10^{-15}$	43.90	$9.60 \cdot 10^{-15}$	70.55	$2.65 \cdot 10^{-14}$
					70.93	$2.09 \cdot 10^{-14}$
Egg tempera	38.15	$1.58 \cdot 10^{-13}$	66.88	$3.09 \cdot 10^{-13}$	58.38	$3.93 \cdot 10^{-13}$
	37.47	$1.41 \cdot 10^{-13}$	66.27	$2.92 \cdot 10^{-13}$	59.60	$3.14 \cdot 10^{-13}$
					59.53	$3.18 \cdot 10^{-13}$
Beeswax	25.40	$2.71 \cdot 10^{-16}$	43.25	$5.32 \cdot 10^{-16}$	72.29	$2.69 \cdot 10^{-16}$
	25.34	$2.25 \cdot 10^{-16}$	44.91	$1.78 \cdot 10^{-15}$	72.22	$3.60 \cdot 10^{-16}$
					72.12	$4.92 \cdot 10^{-16}$

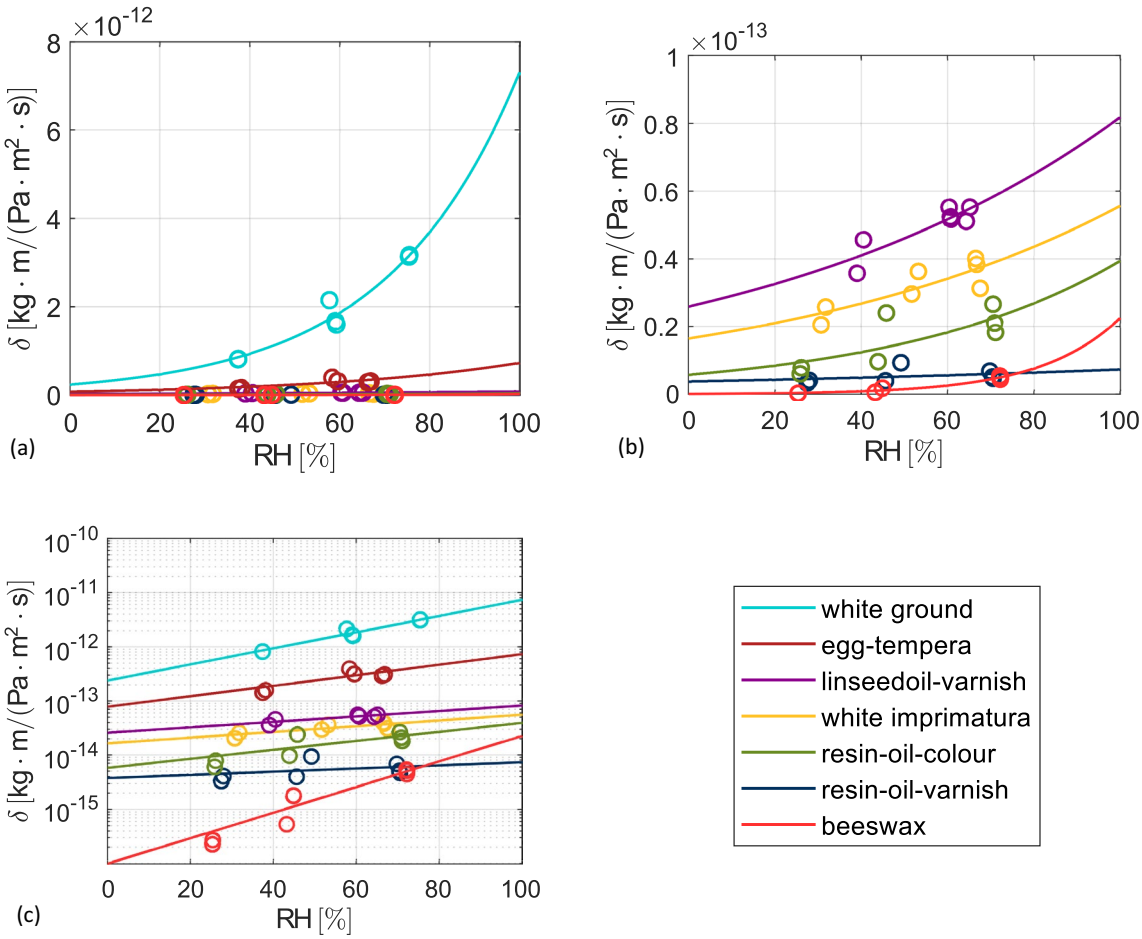

Fig. 9 Comparison of the permeability of the coatings used in the C-series. Experimental values (o) and regression functions (-) plotted in three different scales: (**a**) overall comparison, (**b**) comparison of the coatings with higher resistance and (**c**) logarithmic representation of the permeability

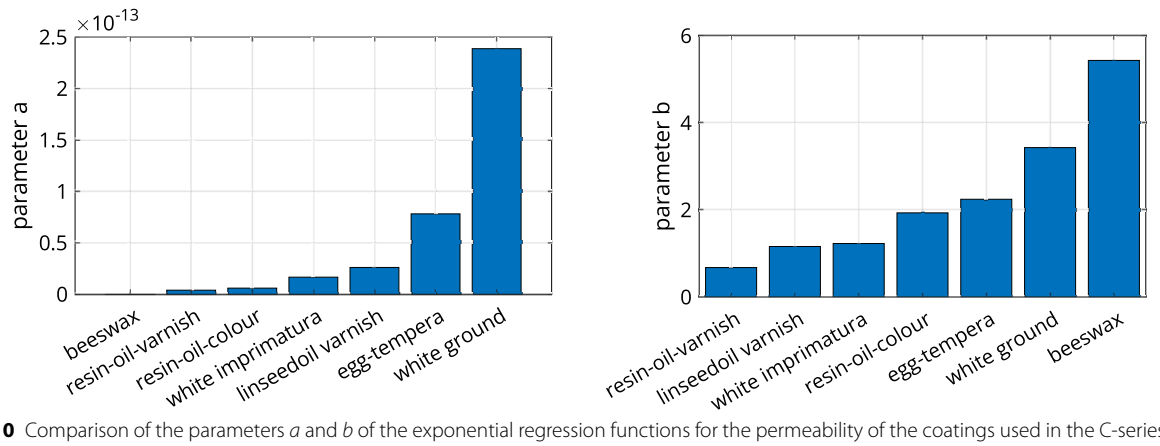

Fig. 10 Comparison of the parameters *a* and *b* of the exponential regression functions for the permeability of the coatings used in the C-series

Table 11 Parameters a_c and b_c of the exponential regression function in Eq. (7) for the permeability of the single coatings used in the C-series, determined from specimens C_{wi}—C_{bw}

Coating	White ground	White imprimatura	Resin oil varnish	Linseedoil varnish	Resin oil colour	Egg tempera	Beeswax
$a_c\left[10^{-15}\frac{\text{kg·m}}{\text{Pa·m}^2\text{·s}}\right]$	254.16	16.734	3.5341	26.053	5.5819	76.634	0.10314
$b_c[-]$	3.3434	1.1696	0.8412	1.1183	2.0112	2.2415	5.3099

The depicted RH-dependent functions represent the permeability of the single coatings applied on a PE frit coated with white ground or directly on the PE frit for white ground. Regarding historical art objects, multiple ground and paint layers are applied on top of each other. Therefore, the total water vapour permeance W_{tot} or resistance Z_{tot} have to be calculated by Eq. (6).

By C_{tot}, a specimen of a PE frit painted with five different coatings is tested. The permeability δ is calculated by Eq. (7) and the resistance by Eq. (5) using the thickness values in Table 8. The resistance of the PE frit is calculated from the water vapour pressure difference and the reference value of the moisture density flow g, see Table 9. Since the distribution of the humidity in the coating system is unknown, δ and Z are determined iteratively. First, the relative humidity has to be estimated to calculate an initial δ and Z. In a next step, the RH difference of each coating can be calculated by $\Delta RH = Z/Z_{tot} \cdot \Delta RH_{tot}$ and, by this, RH, δ and Z can be obtained iteratively. The calculated values can be seen in Table 12.

The total resistance can also be directly determined by the experimental results of the specimens C_{tot} 41, 44 and 45 by $Z_{tot} = \Delta p_{v_{tot}}/g_{tot}$. These values are also shown in Table 12 and are about twice as large as the calculated values. This large difference might occur due to the difficult determination and inhomogeneity of the thickness of the coating layers. There are also transition zones, where two coatings are mixed or one coating penetrates another in the experiments, but are not considered here in the calculations. The effective thickness and, by this, the effective resistance of the coatings would be larger. Therefore, the permeability of coating systems, the interaction of paintings coated on each other and the water transport in transition zones of coatings need to be investigated. Another way to circumvent this issue is to use the consecutive testing strategy as in the following section.

Permeability of the I-series coatings

In contrast to the C-series, and as described in Sect. 2 for the I-series, the different states of the coating system of a specific type of Russian icon after each application step are analysed. Every specimen of the I-series is sliced to determine the average thickness by microscope images. In Fig. 4, two cross-sections can be seen. The mean values of the measured thicknesses as well as relative permeability and permeance, i.e. δ and W, are given in Table 13 for these manufacturing substeps I_1-I_4 at one climate and in Table 14 for the total coating system I_{tot} at three climates. The results as relative and absolute permeability are depicted in Fig. 11. As described in Sect. 3.2.1, the mean RH in the coatings differ also for the same experimental setup.

The results do not allow to give specific material characteristics of the single layers. Thus, it is not reasonable to analyse the relative permeability δ of the investigated composites per thickness of the specimens at the substeps with only some of the layers. Only the total permeance W through the coating system matters.

Table 12 Calculated single and total water vapour resistance and permeance for the coating system C_{tot} obtained by the model and total water vapour resistance and permeance experimentally determined by the C_{tot} specimens No. 41, 44 and 45

	Modelling with parameters obtained by C_{wi}—C_{rv}							Experiment C_{tot}		
	PE frit	White ground	Egg tempera	White imprimatura	Oil colour	Resin oil varnish	Total	Specimen no.		
								41	44	45
Mean RH [-]	0.94	0.94	0.93	0.87	0.79	0.50				
$\delta\left[10^{-14}\frac{\text{kg·m}}{\text{Pa·m}^2\text{·s}}\right]$		613	76	5	3.1	0.56				
$W\left[10^{-10}\frac{\text{kg}}{\text{Pa·m}^2\text{·s}}\right]$	45	152	87	9.5	8.8	1.7	1.2	0.6	0.5	0.6
$Z\left[10^{7}\frac{\text{Pa·m}^2\text{·s}}{\text{kg}}\right]$	22.1	6.59	11.5	105	114	608	867	1760	2020	1680

Table 13 Permeability and permeance and associated relative humidity of the coatings I_1 – I_4 from the I-series calculated from the measured g (RH 0% / 50%)

Coating	Specimen no.	t_{tot} [μm]	RH[%]	$\delta\left[\frac{kg \cdot m}{Pa \cdot m^2 \cdot s}\right]$	$W\left[\frac{kg}{Pa \cdot m^2 \cdot s}\right]$
I_1: S+T	46	150	29.9	$1.19 \cdot 10^{-13}$	$7.96 \cdot 10^{-10}$
	47	100	30.1	$8.40 \cdot 10^{-14}$	$8.40 \cdot 10^{-10}$
	48	120	28.9	$7.22 \cdot 10^{-14}$	$6.02 \cdot 10^{-10}$
	49	120	30.2	$1.04 \cdot 10^{-13}$	$8.69 \cdot 10^{-10}$
I_2: S+T+H	50	150	30.5	$1.39 \cdot 10^{-13}$	$9.27 \cdot 10^{-10}$
	51	200	31.0	$2.07 \cdot 10^{-13}$	$1.04 \cdot 10^{-09}$
I_3: S+T+H+Pr	52	800	29.5	$5.76 \cdot 10^{-13}$	$7.21 \cdot 10^{-10}$
	53	950	29.9	$7.56 \cdot 10^{-13}$	$7.96 \cdot 10^{-10}$
I_4: S+T+H+Pr+Pa+O	54	850	25.4	$4.73 \cdot 10^{-14}$	$5.57 \cdot 10^{-11}$
	55	950	25.4	$5.11 \cdot 10^{-14}$	$5.38 \cdot 10^{-11}$
	56	880	25.4	$5.25 \cdot 10^{-14}$	$5.97 \cdot 10^{-11}$
	57	950	25.4	$5.66 \cdot 10^{-14}$	$5.95 \cdot 10^{-11}$

Table 14 Permeability and permeance and associated relative humidity of the coatings I_5 (S+T+H+Pr+Pa+O+V) from the I-series calculated from the measured g

Climate		t_{tot} [μm]	RH[%]	$\delta\left[\frac{kg \cdot m}{Pa \cdot m^2 \cdot s}\right]$	$W\left[\frac{kg}{Pa \cdot m^2 \cdot s}\right]$
RH 0% / 50%	58	930	25.4	$4.59 \cdot 10^{-14}$	$4.94 \cdot 10^{-11}$
	59	820	25.3	$3.35 \cdot 10^{-14}$	$4.09 \cdot 10^{-11}$
	60	790	25.3	$3.50 \cdot 10^{-14}$	$4.43 \cdot 10^{-11}$
RH 85% / 50%	64	870	66.6	$2.23 \cdot 10^{-13}$	$2.56 \cdot 10^{-10}$
	65	800	66.7	$1.84 \cdot 10^{-13}$	$2.30 \cdot 10^{-10}$
	67	890	66.5	$2.61 \cdot 10^{-13}$	$2.94 \cdot 10^{-10}$
RH 95% / 50%	61	880	70.3	$5.93 \cdot 10^{-13}$	$6.74 \cdot 10^{-10}$
	62	690	70.8	$3.68 \cdot 10^{-13}$	$5.34 \cdot 10^{-10}$
	63	970	71.0	$4.26 \cdot 10^{-13}$	$4.40 \cdot 10^{-10}$

As can be seen in Fig. 11b, the quantity of the total permeance at comparable climate boundary conditions generally decreases by applying further layers and increasing thickness. Unexpectedly, the permeance is increasing after applying the second layer (hardwhite in I_2). The reason for this is not clear to the authors. Probably the production technique (dapping the hardwhite into the freshly applied sizing layer, see "Permeability test specimens for the I-series" Section) changes the composite leading to a new composite different to the sizing material. The strongest resistance gain is obtained by the application of the paint layer and olifa in I_4. By applying the varnish, I_{tot} has, finally, the lowest relative and absolute permeability, compared to the substeps I_1-I_4.

For the total coating system composite I_{tot}, the moisture dependency is analysed by tests in three different climates. In the diagrams on the right of Fig. 11a and b, the RH-dependent permeability is shown, including the fitted exponential functions (Eqs. (7) and (8)) with the parameters given in Table 15.

Although the total coating system is dependent on the material parameters of the single layers, their transition zones in between and the thickness fractions, a relative permeability of the total coating system δ_{tot} in every subtep is given. This approach assumes a coating system characteristic, which allows further material modelling with specific slightly differing thicknesses of coating systems within the numerical analysis of such objects by assuming constant thickness fractions of the single layers. However, this cannot be taken as a general assumption. The permeance is guided by the most resistant layer rather than the total thickness of the whole coating system. In case of unknown thicknesses of the single layers and the quality of the transition zones, it is rather recommended by the authors to model the permeance, i.e. the absolute permeability, without considering the layers' thickness fractions with the RH-dependent function of

$$W_{tot}(RH) = a_W \cdot e^{b_W \cdot RH} \tag{8}$$

Conclusions and Outlook

An investigation of coating systems used for a historical cupboard, a panel painting of L. Cranach the Elder and a Russian icon are conducted. As an outcome of this investigation, characteristic coatings are identified and tested with respect to their permeability. The permeability properties are analysed using the cup method. The measured vapour flow density is translated into a

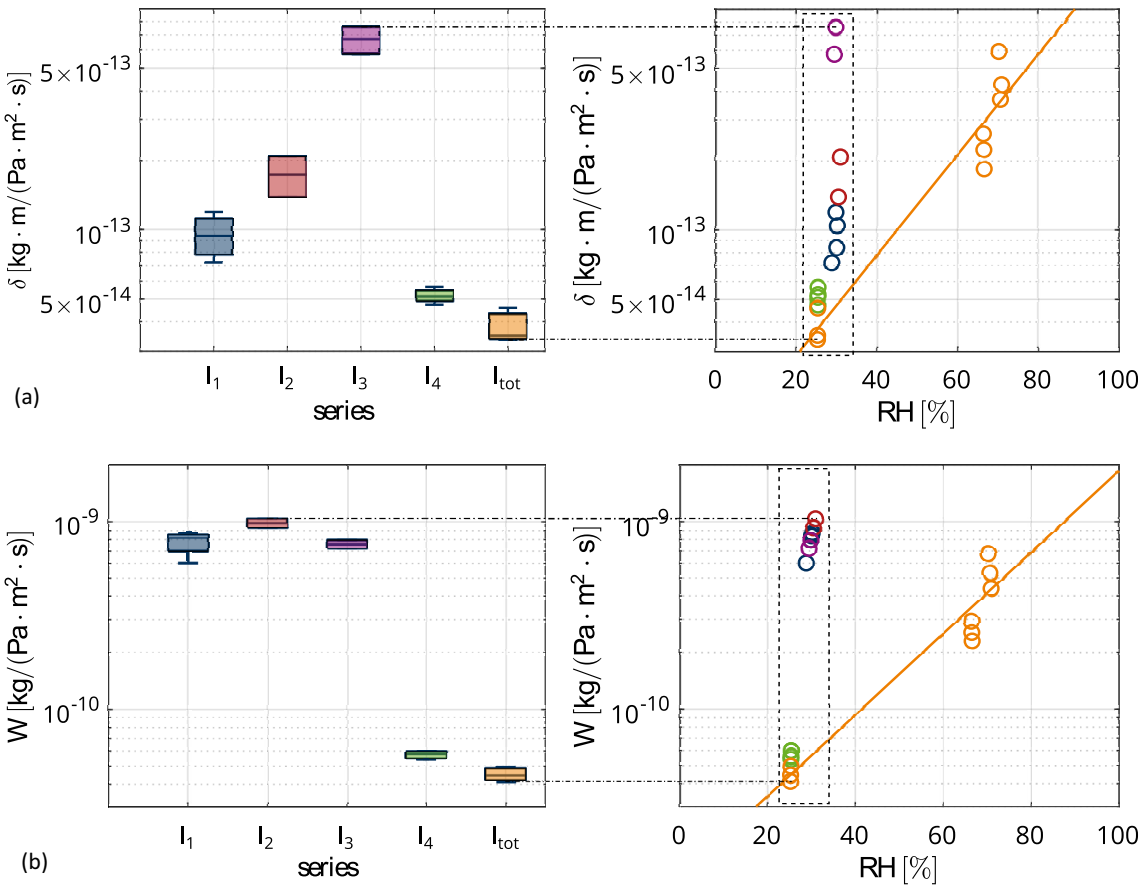

Fig. 11 Comparison of the permeability of the coatings of the I-series: logarithmic boxplot of all investigated layers at cup tests RH 0% / 50%, and experimental values (o) and regression function of total coating system (-) at all cup tests of (**a**) the relative permeability δ and (**b**) permeance W

Table 15 Parameters a and b for the exponential function in Eqs. (7) and (8) for the total coating system of the icon (I_{tot} specimens)

Total permeability/ permeance	$\delta_{tot}=a \cdot e^{b \cdot RH}$	$W_{tot}=a_W \cdot e^{b_W \cdot RH}$
a/a_W	$1.05 \cdot 10^{-14} \frac{kg \cdot m}{Pa \cdot m^2 \cdot s}$	$1.25 \cdot 10^{-11} \frac{kg}{Pa \cdot m^2 \cdot s}$
b/b_W	5	5

layer thickness dependent permeability parameter. Several tests are conducted with different boundary conditions. In this manner, the dependency on the humidity is observed. An exponential function is proposed to model the dependency of the permeability on the relative humidity using two parameters.

Within the investigation of single coating layers in the described C-series, the permeability values of the coatings are compared to each other. For comparison, the model parameter *a*, representing dry material permeability, can be used. The most impermeable coatings are beeswax and resin-containing coatings. White ground and egg tempera are relatively permeable. The parameter *b* of the model represents the moisture dependency of the permeability. The highest moisture dependency is observed for beeswax, followed by white ground, while the varnishes are relatively moisture independent.

The comparison of the results of the summarised single layer and those of the complete coating show differences in permeability. The permeability of the tested total coating system is half as large as the value calculated by the parameters of the single coatings. It is expected that this behaviour is related to the transition zones between the single layers in the total coating system. Also, a transition zone is identified between the painting and the supporting material, which has to be considered when wood replaces the PE frit as the support.

The results of the I-series give selected mechanical and hygric characteristics of the coating system of a special type of Russian icon that enable a hygro-mechanical modelling of these coatings within numerical analyses. The permeability results show the contribution after a stepwise manufacturing process of each additional layer application,

and the total humidity dependent permeability of the total coating system of such panel paintings in the style of Russian icons from the beginning of the twentieth century.

The permeability model parameters are applicable to model coated wooden objects' surface emission and allow to simulate the structural behaviour including water vapour resistance of the coatings.

Further experiments in general and especially in higher humidity ranges are necessary to support the humidity dependent material modelling with more data and to enable an accurate approximation of the water vapour transport behaviour through the investigated layers.

To be able to determine the permeability of a complete coating system composite by the thicknesses and material characteristics of the single layers, further investigations are necessary for the properties of different coating compositions including the transition zones. As can be seen in this study, the water vapour resistance of a coating system cannot be obtained correctly by the summation of the resistances of the single coatings. Therefore, the interaction of coatings needs to be evaluated in order to draw conclusions about coating properties by the properties and thicknesses of the components.

Sorption, swelling and shrinking of the coatings as well as different failure phenomena of coating systems and their associated properties have to be investigated for the damage assessment.

All investigated specimens are tested at an age between one and six months after manufacturing. For many coating materials, an extensive ageing behaviour needs to be stated, see e.g. [4], especially the changing of the mechanical properties, like an increase of stiffness (hardening) and strength. The effect of ageing on the mechanical and hygric characteristics is open to investigation.

The achieved results will be applied in numerical analyses of the herein presented objects in subsequent research. The goal is the risk assessment due to unappropriate climatic conditions and the influence of abrupt climate changes using non-destructive numerical simulations.

Current coating systems for the increasing market of contemporary wooden structures in civil and mechanical engineering and furniture fabrication but also historic coating systems are relevant for more detailed investigations. The properties of coating systems will play an important role in the numerical analysis of historical artwork under climate loading and within preventive conservation.

List of symbols

Abbreviations

C-series: Cranach/cupboard-series; H: Hardwhite; HfBK: Dresden University of Fine Arts; IHD: Institut für Holztechnologie Dresden; ISD: Institute for Structural Analysis; I-series: Icon-series; O: Olifa; Pa: Paintlayer; PE: Polyethylene; Pr: Primer; RH: Relative humidity; S: Sizing; SKD: Dresden State Art Collections; T: Textile; V: Varnish.

Variables

a: Dry water vapour permeability; b: Moisture dependency of δ; d: Damage variable; E: Young's modulus; f: Tension strength; g: Density of water vapour flow rate; p_v: Water vapour pressure; RH: Relative humidity; T: Temperature; t: Thickness; W: Water vapour permeance; w: Width; Z: Water vapour resistance; Δ: Difference; δ: Water vapour permeability; ε: Strain; κ: Damage history; σ: Stress.

Indices

*: Reduced; 0: Initial; bw: Beeswax; c: Coating layer; cr: Crack, complete damage; di: Distemper; et: Egg tempera; in: Inside the cup; lv: Linseedoil varnish; out: Outside the cup; PE: PE frit; rc: Resin oil colour; rv: Resin oil varnish; tot: Total; u: Ultimate; v: Water vapour; wg: White ground; wi: White imprimatura.

Acknowledgements

The authors gratefully acknowledge the support of Institut für Holztechnologie Dresden GmbH for providing the experimental data.

Author contributions

JS, DK, GG, OT, SO and MK design of the work and writing – original draft. GG, OT and SO review of object information, manufacturing of specimens and acquisition of data. JS and DK review of material modelling, analysis and interpretation of data, material modelling. JS, DK, AS and MK conception and writing – review and editing.

Funding

Open Access funding enabled and organized by Projekt DEAL. The described research work is funded by the Federal Ministry of Education and Research (BMBF) within project 03VP05781 "Numerical analysis tool for the simulation and risk estimation of climatic and mechanical loaded works of art made of wood – CultWood" and by the State Ministry of Science and Cultural Affairs of Saxony (SMWK) within project 100371102 "Virtual experiments for artwork – VirtEx".

Availability of data and materials

The datasets used and/or analysed during the current study are available from the corresponding author on request.

Declarations

Competing interests

The authors declare that they have no known competing financial interests or personal relationships that could have appeared to influence the work reported in this paper.

Author details

[1]Institute for Structural Analysis, Technische Universität Dresden, 01062 Dresden, Germany. [2]Dresden University of Fine Arts, Brühlsche Terrasse 1, 01067 Dresden, Germany.

Received: 24 March 2022 Accepted: 30 July 2022
Published online: 08 September 2022

References

1. Hagan E, Quasney E, Mecklenburg MF. A parametric analysis of relative humidity effects on traditional panel paintings. Mater Res Soc Symp Proc. 2005;852:3–11.
2. Mecklenburg MF. Determining the Acceptable Ranges of Relative Humidity And Temperature in Museums and Galleries - Part 1, Structural Response to Relative Humidity. Washington D.C: Smithsonian Conservation Institute; 2007.
3. Rachwał B, Bratasz Ł, Krzemień L, Łukomski M, Kozłowski R. Fatigue damage of the gesso layer in panel paintings subjected to changing climate conditions. Strain. 2012;48:474–81.

4. Froidevaux J. *Wood and paint layers aging and risk analysis of ancient panel painting*. Montpellier: Université Montpellier II; 2012. (PhD Thesis).
5. Lämmlein SL. *Violin Varnishes and Tonewood: Relationships of Vibro-mechanical and Moisture Sorption Properties*. Zürich: ETH Zürich; 2020. (PhD Thesis).
6. Allegretti O, Raffaelli F. barrier effect to water vapour of early European painting materials on wood panels. Stud Conserv. 2008;53:187–97.
7. Hagenmaier R, Shaw PE. Permeability of shellac coatings to gases and water vapor. J Agric Food Chem. 1991;39:825–9.
8. Lämmlein SL, Mannes D, van Damme B, Schwarze FW, Burgert I. The influence of multi-layered varnishes on moisture protection and vibrational properties of violin wood. Sci Rep. 2019;9:18611.
9. De Backer L, Laverge J, Janssens A, De Paepe M. Evaluation of the diffusion coefficient and sorption isotherm of the different layers of early Netherlandish wooden panel paintings. Wood Sci Technol. 2018;52:149–66.
10. Ruus A, Peetsalu P, Tohvri E, et al. Water vapour transmission properties of natural paints. Agronomy Res Biosystem Eng Special Issue. 2011;1:197–201.
11. Hendrickx R, Desmarais G, Weder M, Ferreira ESB, Derome D. Moisture uptake and permeability of canvas paintings and their components. J Cult Herit. 2016;19:445–53.
12. Bosco E, Suiker A, Fleck NA. Crack channelling mechanisms in brittle coating systems under moisture or temperature gradients. Int J Fract. 2020;225:1–30.
13. Bosco E, Suiker A, Fleck NA. Moisture-induced cracking in a flexural bilayer with application to historical paintings. Theoret Appl Fract Mech. 2021;112: 102779.
14. Ritz G, Schmidt-Glassner H. Alte bemalte Bauernmöbel. 3rd ed. München: Georg D.W. Callwey; 1980.
15. Ottenjann H. *Farbige volkstümliche Möbel*. Cloppenburg: Museumsdorf Cloppenburg; 1982.
16. Sacher J. Studien zur Bemalung der sogenannten Herrnhuter Möbel. In: *Beiträge zur Erhaltung von Kunstwerken*. Berlin: Restauratoren Fachverband; 1997.
17. Marx H, Giebe M. *Lukas Cranach der Ältere, der linke Flügel (Innenseite) des Katharinenaltars von 1506*. Dresden: Kulturstiftung der Länder; 1996.
18. Heydenreich G. Lucas Cranach the Elder: Painting materials, techniques and workshop practice. Amsterdam: Amsterdam University Press; 2007.
19. Gebhardt C, Konopka D, Börner A, Mäder M, Kaliske M. Hygro-mechanical numerical investigations of a wooden panel painting from "Katharinenaltar" by Lucas Cranach the Elder. J Cult Herit. 2018;29:1–9.
20. Herm C, Tietze O, Belik Z, Konopka D, Trufanova O, Fuhrmann A, Weiß B, Kaden J, Kaliske M. The Icon Last Supper of the Iconostasis of the Russian Memorial Church in Leipzig: technological investigation as basis for the modelling and the numerical simulation of historical works of art. Studies Conser. 2021. https://doi.org/10.1080/00393630.2021.1940021.
21. Шнейдер И, Федоров П. Техника иконописи. Руководство к практическому изучению писания православных икон по приемам первых иконописцев. In: *Общество «Икона» в Париже*. Москва: Прогресс-Традиция; 2002. p. 241–280.
22. Espinola VBB. Russion icons: spiritual and material aspects. J Am Inst Conserv. 1992;31:17–22.
23. Weissmann G. Techniques of Traditional Icon Painting. Tunbridge Wells: Search Press Ltd; 2012.
24. Konopka D, Kaliske M. Inside the icon: experimental and numerical analysis of climate impacts on the damage potential of panel paintings. In: Kaliske M, Konopka D, Tietze O, Herm C, editors. Virtual Experiments for Wooden Artwork. Dresden: Technische Universität Dresden; 2021. p. 42–57.
25. Wehlte K. Werkstoffe und Techniken der Malerei. Ravensburg: Otto Maier Verlag; 1967. p. 645.
26. Schulze A. Goldleder zwischen 1500 und 1800: Herstellung und Erhaltung. Dresden: Sax-Verlag; 2011.
27. Kelm C, Eisbein M. *Restaurierungsdokumentation zum Flügelaltar von Lucas Cranach dem Älteren, 1539*. Dokumentationsarchiv des Landesamtes für Denkmalpflege Sachsen; 1996.
28. DIN EN 408:2012–10. *Holzbauwerke - Bauholz für tragende Zwecke und Brettschichtholz - Bestimmung einiger physikalischer und mechanischer Eigenschaften*. Berlin: Beuth-Verlag; 2012.
29. Tietze O, Maximova G, Konopka D, Sharova N, Kaliske M. The Production of Technological Replicas of an Icon and Test Specimens as Part of the Project "Virtual Experiments for Artwork." Zeitschrift für Kunsttechnologie und Konservierung. 2021;34:378–97.
30. Lemaitre J. A continuous damage mechanics model for ductile fracture. J Eng Mater Technol. 1985;107:83–9.
31. DIN EN ISO 12572:2016. *Wärme- und feuchtetechnisches Verhalten von Baustoffen und Bauprodukten - Bestimmung der Wasserdampfdurchlässigkeit - Verfahren mit einem Prüfgefäß (ISO 12572:2016)*. Berlin: Beuth-Verlag; 2016.
32. DIN EN ISO 7783:2018. *Beschichtungsstoffe - Bestimmung der Wasserdampfdurchlässigkeit*. Berlin: Beuth-Verlag; 2018.
33. Konopka D, Bachtiar EV, Niemz P, Kaliske M. Experimental and numerical analysis of moisture transport in walnut and cherry wood in radial and tangential material directions. BioResources. 2017;12:8920–36.
34. Hering S, Keunecke D, Niemz P. Moisture-dependent orthotropic elasticity of beech wood. Wood Sci Technol. 2011;46:927–38.
35. Möller B, Graf W, Beer M. Fuzzy structural analysis using α-level optimization. Comput Mech. 2000;26:547–65.

Publisher's Note